Hindawi
Mathematical Problems in Engineering
Volume 2018, Article ID 8909031, 16 pages
https://doi.org/10.1155/2018/8909031

Research Article

Fault Diagnosis of Wheel Flat Using Empirical Mode Decomposition-Hilbert Envelope Spectrum

Hua Jiang [1,2] **and Jianhui Lin** [2]

[1] *School of Information Science and Technology, Southwest Jiaotong University, Chengdu 610031, China*
[2] *State Key Laboratory of Traction Power, Southwest Jiaotong University, Chengdu 610031, China*

Correspondence should be addressed to Hua Jiang; jhtgzyyx@163.com

Received 15 August 2018; Revised 4 October 2018; Accepted 24 October 2018; Published 18 December 2018

Academic Editor: Stefano Sfarra

We establish the Injury Model of Wheel Flats with 10 degrees of freedom and calculate the dynamic responses of the railway vehicle system, which include different vehicle speeds and different length flats. The Hilbert envelope spectrum method based on Empirical Mode Decomposition (EMD) is proposed according to the nonstationary characteristics of axle box acceleration (ABA) signal. The vibration characteristics of the ABA are studied thoroughly. And then the effects concerning speed and flat length on the diagnosis results are analyzed. The simulation results show the amplitude corresponding to the frequency component of wheel flats raise with the increasing of the wheel flat length when the single or double wheel flats impact the track at the same vehicle speed. In other words, the longer the wheel flat is, the greater the magnitude of the decomposition result is. In the same vehicle speed, the amplitude corresponding to the frequency component of wheel flat is minimum when the two flats' phase difference is 180°. With the same flat length (single or double wheel flats), the amplitude corresponding to the frequency components of wheel flats decreases with the increasing of the speed. This method could accurately and effectively identify the frequency of wheel flats.

1. Introduction

Wheel flat is a common and difficult problem to be solved in the world. With the railway trains speed-up in China, the wheel flats problem is more serious. The wheel flats bring the intermittent impact and injury to the rail and sleeper. The wheel flats not only affect riding comfort and safety but also bring trouble to the maintenance of the line. A large number of studies have shown that the wheel-rail force caused by wheel flat increases heavily with the improving speed of vehicle. The growth is linear at the 60~90 km/h speed range [1–4]. In addition, the wheel flat will be deteriorated further because of the wheel-rail impact.

Many condition monitoring systems for detecting the railway wheel defects had been developed [5–38]. The available condition monitoring systems are divided into inworkshop and inservice inspection. The inservice inspection is divided into onboard measurement and wayside measurement. The inworkshop inspection system can be divided into ultrasonic techniques [7–11], infrared and thermography inspection [12–15], and magnetic methods [16–18] according to the selected sensors. These methods are mostly used for detecting wheel crack. Some methods need special equipment, which is not suitable for inservice monitoring.

There are many monitoring systems for inservice and wayside inspections. These technologies are usually used, such as train gauges [19], fibre Bragg Grating sensor [20], vibration technique [21–24], and acoustic technique [25]. There are many parameters to be measured, such as surface defects [19, 20], subsurface defects [23] of wheel set, derailment coefficient [19], dynamic load, and static load (weight of train) [20]. Transducers are arranged on or nearby the track using monitoring systems for inservice and wayside inspections. Thus, they are incapable of real-time detection of the vehicle running state in the process. The deficiencies of wayside monitoring can be overcome using onboard inspections. Inservice and onboard inspections are becoming popular increasingly in an attempt to improve the quality and efficiency of vehicle condition monitoring and fault diagnosis.

The monitoring systems for inservice and onboard inspections usually adopted ultrasonic technique [26], acoustic technique [27], vibration technique [2, 28–31] and magnetic technique [32] to detect flange contact [26], surface defects of wheel-set [26–30], and derailment coefficient [32], respectively. Liang et al. analyzed the vibration signals and acoustic signals stimulated by the wheel flat and rail surface defects at different speeds levels [29]. Because the original signal is completely buried by stronger background reverberating acoustic noise, when the wheel speed is high, the acoustic signal cannot effectively determine the defects. In addition, the noise detection method cannot overcome the interference from adjacent wheel.

Chen et al. defined the generalized energy based on Empirical Mode Decomposition (EMD) and analyzed the simulated track vibration signal [33]. Chen used the empirical energy threshold to detect wheel flat. The threshold value directly affected the detection rate of flat. Li et al. adopted the improved EMD to solve the problem of modal aliasing [34]. The axle box acceleration signal was analyzed by this method, and the effect was better than that of Ensemble Empirical Mode Decomposition (EEMD).

The vibration acceleration detection method is more reliable and has better detection effect. In terms of applicability, the axle box acceleration (ABA) detection method is easy to install and low in cost. And this method is suitable for both the high and low train speed at the same time and can be used for onboard real-time monitoring. However, vehicle track coupling system is nonlinear. When the vehicle system is stimulated by the random irregularity of track, the wheel flat and rail defects will cause the vibration impact of vehicle system, so the ABA is nonstationary and nonlinear.

Because ABA is nonlinear and nonstationary, FFT cannot be applied. The ABA signal is windowed into short-time interval stationary (pseudo-stationary) through Short-time Fourier transform (STFT), but STFT has a single resolution, which is very disadvantageous to analyze. Although wavelet transform solves the problem of single resolution of STFT, it needs to predefine the wavelet base and set the decomposition level. In addition, wavelet transform is suitable for linear signal, and it is easy to produce false harmonics for nonstationary signals, so it is not suitable for nonlinear signal. For nonlinear nonstationary signals, the commonly used decomposition methods are iterative filtering (IF) [35]. The IF algorithm requires setting a low pass filter function in advance. This setting can effectively reduce noise interference, but for nonstationary and nonlinear signals, fixed filter will lead to waveform distortion, poor adaptability, and other issues. Antonio Cicone et al. proposed adaptive local iterative filtering [36]. Another decomposition method for nonlinear and nonstationary signals is EMD. This method is chosen in this paper. For different signals, empirical mode decomposition can select the basis function adaptively according to the original signal, and EMD has good decomposition ability for nonlinear signals [37, 38].

When the wheel tread is faulty, the periodic rotation of wheel will cause periodic nonlinear impulse impact force, resulting in the modulation of vibration signals. Therefore, in this paper, a Hilbert envelope spectrum method based on EMD is proposed to extract modulation information and analyze the potential fault information of wheel flat. The paper is presented as follows. In Section 2, the Injury Model of Wheel Flats with 10 degrees of freedom is established. Section 3 introduces basic concepts for the Hilbert envelope spectrum based on EMD. In Section 4, the ABA signals with different speed, different length of flat, and different phase difference are analyzed, and the influence of these parameters on the decomposition results is discussed. Finally conclusions are given in Section 5.

2. The Vehicle-Track Model

The injury model of wheel flats with 10 degrees of freedom has been established. This model is coupled with the three-layer track model. Considering vertical monorail excitation, the model adopts parameters of quasi high speed passenger car (QHSC).

A half-vehicle vertical system model consists of car body, bogie, primary suspensions, second suspensions, and wheelsets. It is shown in Figure 1 [6]. The vehicle system is regarded as a multirigid body system with a speed of $\boldsymbol{V}$. The vehicle system has ten degrees of freedom such as the ups and downs of car body $\mathbf{Z_c}$, nod of car body β_c, the ups and downs of front and rear frames $\mathbf{Z_{ti}}(\mathbf{i=1,2})$, nods of front and rear frames $\boldsymbol{\beta_{ti}}(\boldsymbol{i = 1,2})$, and vertical vibration of four wheelsets $\mathbf{Z_{wi}}(\mathbf{i=1 \sim 4})$.

Spring-damping vibration model includes three layers (rail-sleeper-ballast-subgrade). It is established in the track part. The rail is considered as continuous infinite Euler beam which is supported by elastic discrete points. The foundation under rail is separated along the longitudinal direction. Each sleeper fulcrum is a discrete unit and each supporting unit adopts double mass (sleeper quality $\mathbf{M_{si}}$ and ballast quality $\mathbf{M_{bi}}$). The relevant model parameters are listed in literature [39].

By Hertz nonlinear elastic contact theory, vertical forces of wheel-rail can be determined:

$$\boldsymbol{p}(\boldsymbol{t}) = \left[\frac{\mathbf{1}}{\boldsymbol{G}}\boldsymbol{\delta Z}(\boldsymbol{t})\right]^{3/2} \tag{1}$$

In formula (1), $\boldsymbol{G}$ is contact constant of wheel-rail, and $\boldsymbol{\delta Z}(\boldsymbol{t})$ is elastic compression of wheel-rail. Then, the vertical coupling relationship between vehicle and track is established, i.e.,

$$\boldsymbol{p_j}(\boldsymbol{t}) = \begin{cases} \left\{\frac{\mathbf{1}}{\boldsymbol{G}}\left[\boldsymbol{Z_{wj}}(\boldsymbol{t}) - \boldsymbol{Z_r}\left(\boldsymbol{x_{wj}}, \boldsymbol{t}\right) - \boldsymbol{Z_0}(\boldsymbol{t})\right]\right\}^{3/2} \\ \mathbf{0} \quad \boldsymbol{\text{wheel separates themself from track}} \end{cases} \tag{2}$$

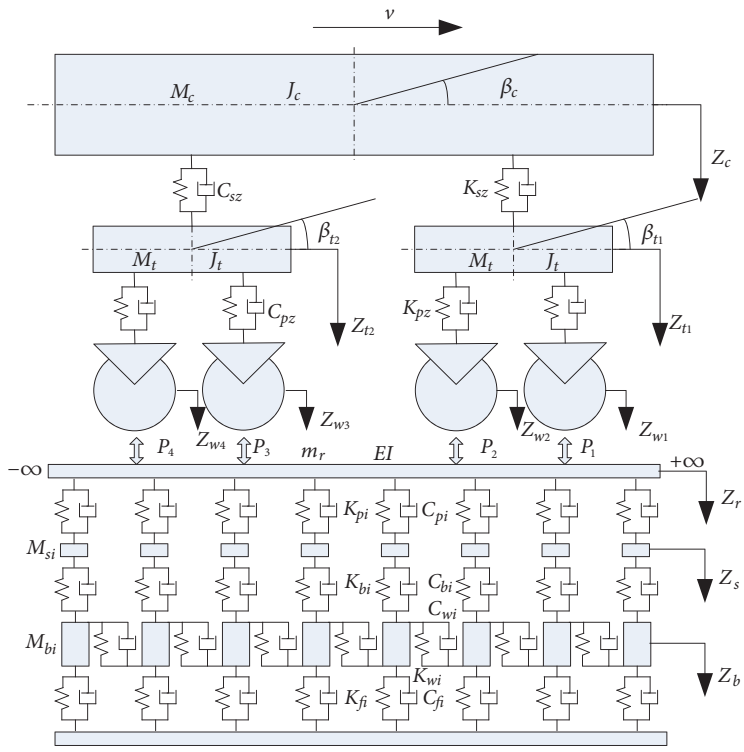

Figure 1: Vehicle-track vertical coupling system model.

When wheel and rail contact, the elastic compression of wheel-rail is determined by the displacement of wheel and rail. In formula (2), $\boldsymbol{Z_{wj}(t)}$ is the displacement of jth wheel, $\boldsymbol{Z_r(x_{wj}, t)}$ is the displacement of rail under jth wheel at time $\boldsymbol{t}$, and $\boldsymbol{Z_0(t)}$ is the track irregularity. When wheel separates themself from track, $\boldsymbol{\delta Z(t) < 0}$, the wheel-rail force is zero. It is known that vehicle-track coupling system is a nonlinear system from formula (2).

In the model, the rail irregularity consists of two parts. One is wheel flat, the other is random irregularity of track, which is the American six-grade track irregularity [40] and simulated by Inverse Fast Fourier Transform (IFFT) method. Generally, the irregularity function of a wheel flat can be described by the cosine curve. The formula (3) was proposed by Lyon [3] to describe rounded flats:

$$\mathbf{Z_{01}}=\frac{\mathbf{1}}{\mathbf{2}}\mathbf{D_f}\left[\mathbf{1}-\mathbf{cos}\left(\frac{\mathbf{2\pi x}}{\mathbf{L}}\right)\right] \tag{3}$$

In formula (3), $\boldsymbol{L}$ is the length of flat. $\boldsymbol{D_f}$ is the valid flat depth. $\boldsymbol{D_f}$ may be estimated through formula (4), and $\boldsymbol{R}$ is the wheel diameter.

$$\boldsymbol{D_f} = \frac{\boldsymbol{L^2}}{\boldsymbol{16R}} \tag{4}$$

The dynamic equations of vehicle-track coupling system are unified into $[\mathbf{M}]\{\ddot{\mathbf{X}}\}+[\mathbf{C}]\{\dot{\mathbf{X}}\}+[\mathbf{K}]=\{\mathbf{P}\}$. ***[M], [C], [K]*** are the mass, damping and stiffness matrices of the vehicle-track coupling system respectively. $\{\mathbf{X}\}$ is the generalized displacement vector, $\{\dot{\mathbf{X}}\}$ is the generalized velocity vector, $\{\ddot{\mathbf{X}}\}$ is the generalized acceleration vector, and $\{\boldsymbol{P}\}$ is a generalized load vector. The new explicit integral method [6] is used to solve the established injury model of wheel flat. The ABA can be obtained by the model.

3. Method of Analysis

The vibrations of a vehicle with wheel flats usually have a periodic impulse force, which leads to a modulation phenomenon of the vibration signal. Moreover, the ABA signal of a vehicle has nonlinear and nonstationary characteristics. By the demodulation method, the modulation information is extracted from the signal, and the strength and frequency of the signal can be analyzed to identify the fault of wheel flat effectively.

After a thorough study of the concept of instantaneous frequency, Hilbert-Huang Transform (HHT) is founded by Norden, E., and Huang et al. [37, 38]. The concept of Intrinsic Mode Functions (IMFs) and the method of decomposing arbitrary signals into IMFs are proposed in Empirical Mode Decomposition (EMD) method. Reasonable definitions, physical meaning, and solution of instantaneous frequency are also given in this method.

An IMF is a function which has the characteristic of having the same numbers of zero-crossings and extreme points, and also having symmetric envelops defined by local maxima and minima respectively.For non-stationary data, the local mean is calculated by the local time scale. In EMD decomposition, local symmetry is replaced by the mean value of envelope determined by local maximum and

local minimum respectively. In the definition of the IMF, IMF is not limited to narrowband signals. IMF may also be amplitude or frequency modulation. It is also the continuous intrinsic mode of this frequency.

EMD is often referred to as a sifting process. According to adaptive characteristics of this sifting process, an arbitrary signal is decomposed into a series of IMF $\mathbf{C_i}$. The remainder is $\mathbf{r_n}$. So the original signal could be expressed by $\mathbf{x(t)}=\sum_{i=1}^{n}\mathbf{C_i}+\mathbf{r_n}$. According to the definition of the IMF, $\boldsymbol{C_i}$ is a narrow band signal.

And then, there is a narrow band signal $\boldsymbol{C_i}$,

$$\mathbf{C_i}(\mathbf{t}) = \mathbf{a_i}(\mathbf{t})\cos\left[2\pi\mathbf{f_{ci}}\mathbf{t} + \boldsymbol{\varphi}_\mathbf{i}(\mathbf{t})\right] \tag{5}$$

where $\mathbf{f_{ci}}$ is the carrier frequency, $\mathbf{a_i(t)}$ is the envelope of $\mathbf{C_i(t)}$, and $\boldsymbol{\varphi_i(t)}$ is the phase of $\mathbf{C_i(t)}$. Because $\mathbf{C_i(t)}$ is a narrow band signal, $\mathbf{a_i(t)}$ is also a narrow band signal. So $\mathbf{a_i(t)}$ can be set to

$$\mathbf{a_i}(\mathbf{t}) = \left[\mathbf{1} + \sum_{\mathbf{m=1}}^{\mathbf{M}} \mathbf{X_{mi}}\cos\left(2\pi\mathbf{f_{mi}}\mathbf{t} + \boldsymbol{\gamma}_{\mathbf{mi}}\right)\right] \tag{6}$$

In formula (6), $\mathbf{f_{mi}}$ is the frequency component of the amplitude modulation signal $\mathbf{a_i(t)}$. And $\boldsymbol{\gamma}_{\mathbf{mi}}$ is the initial phase angle of $\mathbf{a_i(t)}$.

By taking the Hilbert Transform of each IMF component $\boldsymbol{C_i(t)}$, the analytic signal $\boldsymbol{y_i(t)}$ is obtained, i.e.,

$$\begin{aligned}\mathbf{y_i}(\mathbf{t}) &= \mathbf{C_i}(\mathbf{t}) + \mathbf{j}\mathscr{H}\left[\mathbf{C_i}(\mathbf{t})\right] \\ &= \boldsymbol{e}^{j[2\pi f_{ci}t+\varphi_i(t)]}\left[\mathbf{1} + \sum_{m=1}^{M} \boldsymbol{X}_{mi}\cos\left(2\pi f_{mi}t + \gamma_{mi}\right)\right]\end{aligned} \tag{7}$$

If $\boldsymbol{Y_i(t)} = \mathbf{1} + \sum_{m=1}^{M} \boldsymbol{X}_{mi}\cos(2\pi f_{mi}t + \gamma_{mi})$ and $\boldsymbol{\Phi_i(t)} = 2\pi f_{ci}t + \varphi_i(t)$

then analytic signal can be reexpressed as

$$\boldsymbol{y_i}(\boldsymbol{t}) = \boldsymbol{Y_i}(\boldsymbol{t})\,\boldsymbol{e}^{j\Phi_i(t)} \tag{8}$$

It can be seen from the formula (5), that is,

$$\boldsymbol{a_i}(\boldsymbol{t}) = \boldsymbol{Y_i}(\boldsymbol{t}) = \sqrt{\left[\boldsymbol{C_i}(\boldsymbol{t})\right]^2 + \left[\mathscr{H}\left[\boldsymbol{C_i}(\boldsymbol{t})\right]\right]^2} \tag{9}$$

$$\begin{aligned}\boldsymbol{\varphi_i}(\boldsymbol{t}) &= \boldsymbol{\Phi_i}(\boldsymbol{t}) - 2\pi\boldsymbol{f_{Ci}}\boldsymbol{t} \\ &= \arctan\left(\frac{\mathscr{H}\left[\boldsymbol{C_i}(\boldsymbol{t})\right]}{\boldsymbol{C_i}(\boldsymbol{t})}\right) - 2\pi\boldsymbol{f_{Ci}}\boldsymbol{t}\end{aligned} \tag{10}$$

It shows that Hilbert transform could be used to solve the analytic signal for narrowband signals. Then the amplitude demodulation of the signal $\mathbf{a_i(t)}$ and phase demodulation $\boldsymbol{\varphi}_\mathbf{i}(\mathbf{t})$ can be obtained. The frequency demodulation can be solved from the following:

$$\mathbf{f_i}(\mathbf{t}) = \frac{\mathbf{1}}{\mathbf{2\pi}}\frac{\mathbf{d}\boldsymbol{\varphi}}{\mathbf{dt}} = \frac{\mathbf{1}}{\mathbf{2\pi}}\frac{\mathbf{d}\boldsymbol{\Phi}(\mathbf{t})}{\mathbf{dt}} - \mathbf{f_{ci}} \tag{11}$$

Vehicle system is stimulated by the random irregularity of track and wheel flat simultaneously, so the vibration response curve contains many intrinsic modes. Therefore, the ABA signal is decomposed by EMD, and the intrinsic modes $\boldsymbol{C_i(t)}$ are obtained. Comparing with (3) and (6), it can be found that the irregularity function of wheel flat $\boldsymbol{Z_{01}}$ and the amplitude envelop of IMF function $\boldsymbol{C_i(t)}$ have the same form. That is to say, in the intrinsic mode $\boldsymbol{C_i(t)}$ of the wheel flat, $\boldsymbol{a_i(t)}$ is the amplitude envelope of the vibration response caused by the flat irregularity function, and $\boldsymbol{f_{ci}}$ is the natural frequency of the vehicle system. Therefore, we could extract the information of the wheel flat contained in the vibration signal by the Hilbert demodulation method based on EMD.

The steps of the Hilbert envelope spectrum based on the EMD are obtained as follows:

(1) The original signal $\mathbf{x(t)}$ is decomposed by EMD, and the narrow band signal $\boldsymbol{C_i(t)}$ is obtained.

(2) Each IMF component $\boldsymbol{C_i(t)}$ is transformed by Hilbert Transform.

(3) The analytic signal $\mathbf{y_i(t)}$ can be obtained by taking $\boldsymbol{C_i(t)}$ as the real parts and taking the Hilbert Transform of $\boldsymbol{C_i(t)}$ as imaginary parts, i.e. $\mathbf{y_i(t)}=\mathbf{C_i(t)}+\mathbf{j}\mathscr{H}[\mathbf{C_i(t)}]$.

(4) Obtain the amplitude of the analytic signal $\mathbf{y_i(t)}$ to get the envelope of the signal.

(5) The envelope is filtered through low pass and fast Fourier transform. The envelope spectrum is obtained. Then modulation frequency and its high-order harmonics are achieved. So the phase modulation function is also obtained.

4. Analysis and Discussion

4.1. Single Wheel Flat

4.1.1. Identification of Wheel Flat with Different Lengths. Using the vehicle-track model, the vertical ABAs of the vehicle are calculated at different flat lengths.

The vertical acceleration response curves stimulated by different length flats (10mm, 20mm, 30mm, 40mm, and 50mm) is shown in Figure 2(a) and there is no orbital excitation. At the same time, the longer the wheel flats is at the same vehicle speed and the greater the ABA is. The maxima of ABA stimulated by different length flats are shown in Figure 2(b). In the absence of orbit disturbance, the maxima of ABAs are proportional to the lengths of the wheel flat.

However, as the vehicle system is running, it is not only impacted by the wheel flats, but also by the disturbance of the track. When the speed is 100km/h, the vertical ABA response curves stimulated by different length wheel flats and the American six-grade track irregularity are shown in Figure 3. The track irregularity is simulated using the PSD of American six-grade track irregularity [40] by the IFFT method. The wheel diameter is 0.915m, and the theoretical frequency is 9.6633Hz. Similar to the nonorbital excitation, the maximum amplitudes of the ABA increase with the growth of the wheel flat lengths.

From Figures 2(a) and 3, it can be found that the maximum of ABA is equivalent to that of random track irregularity when the length of wheel flat is 10mm. So we can

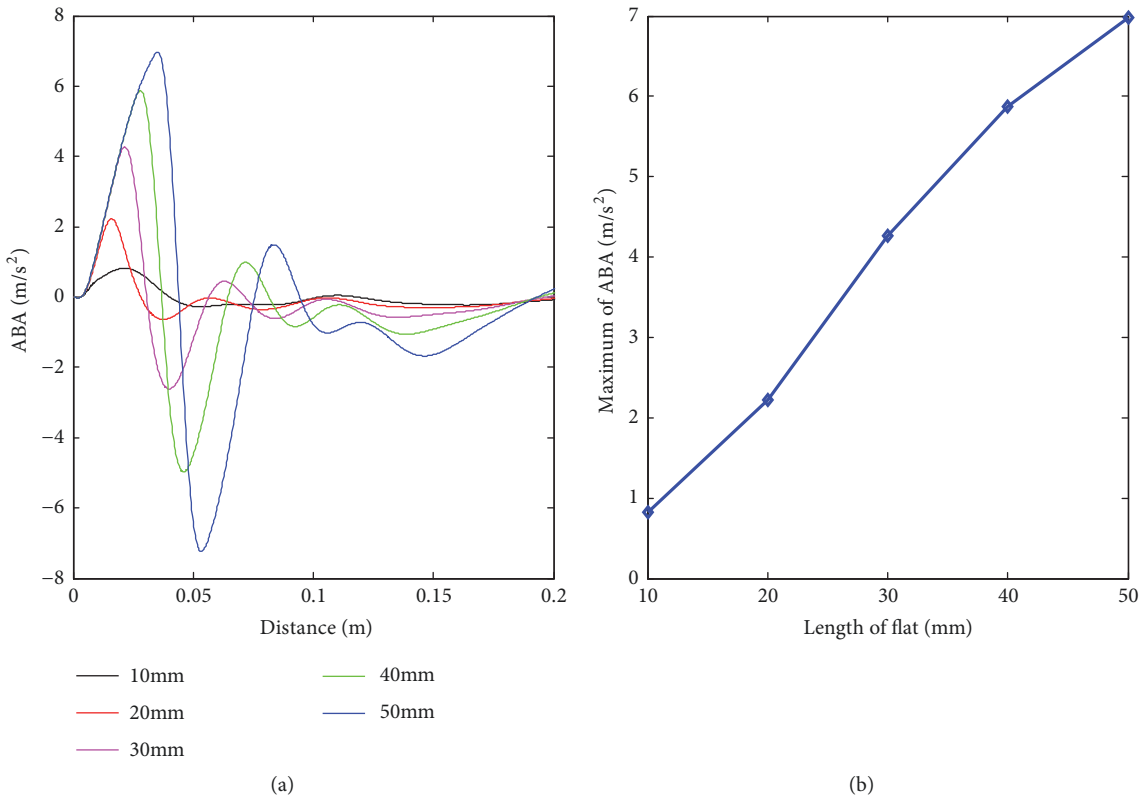

FIGURE 2: Vertical ABA with different length wheel flats and no orbit disturbance (V=100km/h) (a) vertical ABA curve (b) maxima of ABA.

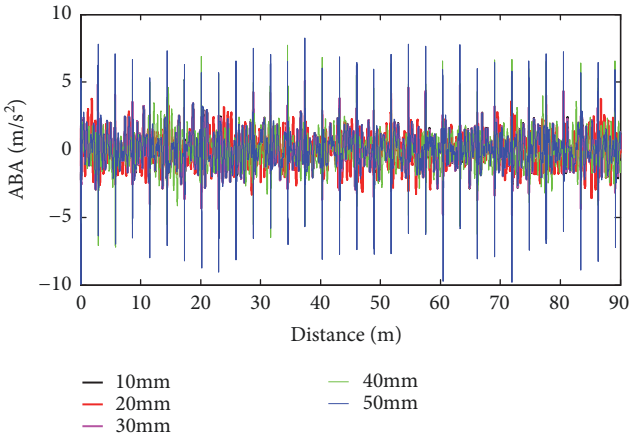

FIGURE 3: Vertical ABA with different wheel flat lengths and American six-grade track irregularity (V=100km/h).

conclude that the vibration caused by flat scar is submerged in the vibration caused by random track irregularity, when the length of wheel flat scar is small. If the noise is added, the vibration frequency of the flat scar would be submerged, and the vibration characteristics caused by the flat scar cannot be effectively identified. For the sake of space, the decomposition result of EEMD is not given here.

The acquired ABA signals are decomposed by EMD to get narrow band random signal $\mathbf{IMF_i}$. The Hilbert envelope spectrums of $\boldsymbol{IMF_1}$ containing vibration information are shown in Figure 4(a). The sums of $\boldsymbol{IMF_1}$-$\boldsymbol{IMF_3}$ Hilbert envelope spectrums obtained from the decomposition of the vibration signal are shown in Figure 4(b). It is concluded that the ideal decomposition results could be obtained when the lengths of the wheel flat are different. The corresponding wheel flat frequencies, as shown in Table 1, are all fluctuating near the theoretical frequency. Both the amplitude of Hilbert envelope spectrum of $\boldsymbol{IMF_1}$ and the sum of Hilbert envelope spectrum amplitudes of the first three intrinsic modes increase with the growth of flat lengths. Effects of flat length on Hilbert envelope spectrum amplitude are shown in Figure 5.

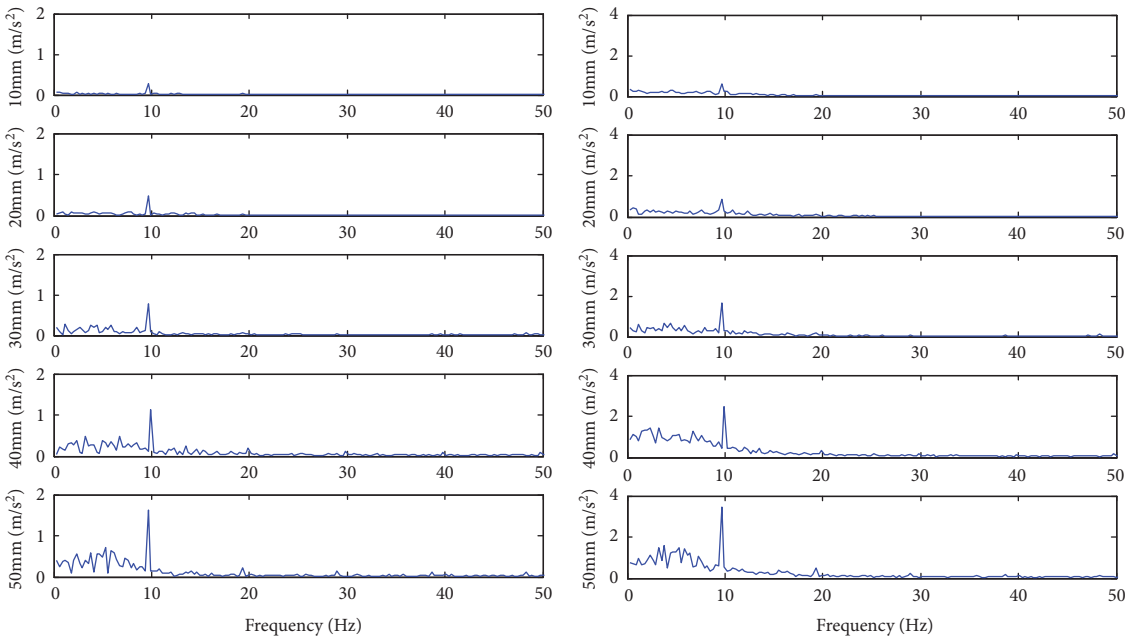

Figure 4: Hilbert envelope spectrum based on EMD with single flat having different lengths. (a) Hilbert envelope spectrum of IMF1 with different length flats. (b) The sum of Hilbert envelope spectrum of IMF1-IMF3 with different length flats.

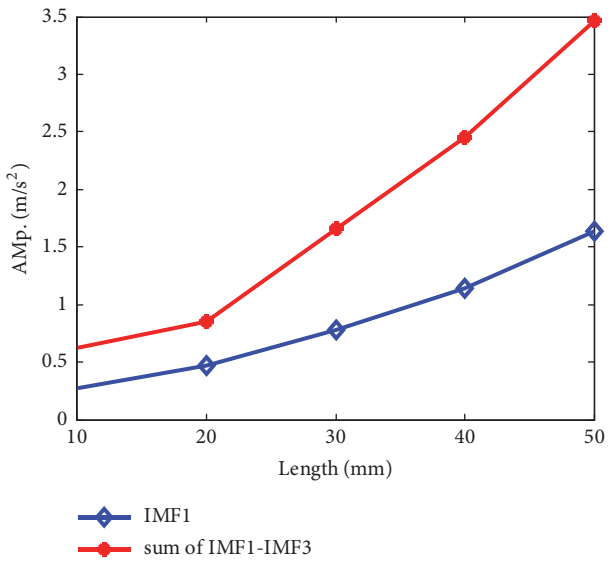

Figure 5: Effects of flat length on Hilbert envelope spectrum amplitude with single flat.

Table 1: Effects of flat length on Hilbert envelope spectrum amplitude with single flat.

Flat length (mm)	Actual frequency (Hz)	Amplitude of IMF1Hilbert envelope spectrum (m/s^2)	Sum of Hilbert envelope spectrum amplitude of IMF1-IMF3 (m/s^2)
10	9.663	0.2771	0.6241
20	9.663	0.4736	0.8563
30	9.661	0.7822	1.6616
40	9.659	1.1364	2.4500
50	9.659	1.6320	3.4636

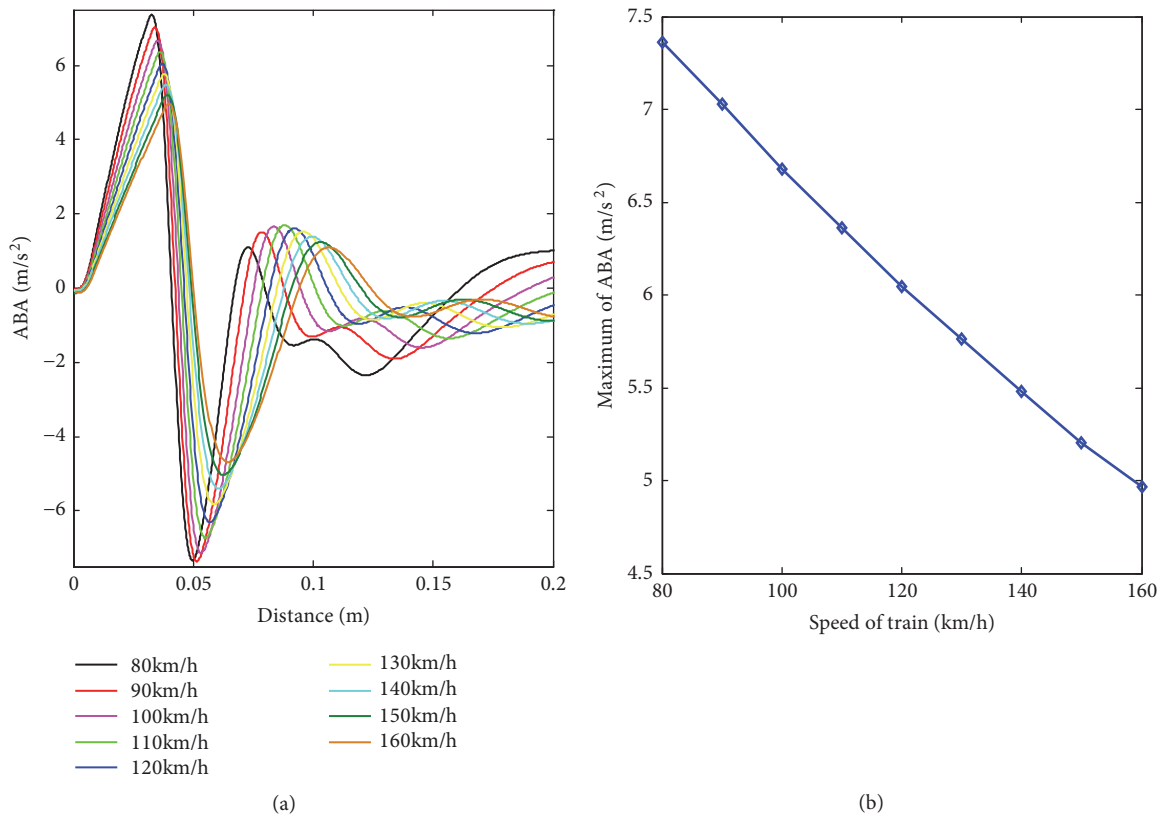

Figure 6: Vertical ABA at different vehicle speeds and no orbit disturbance (length of flat=50mm) (a) vertical ABA curve (b) maxima of ABA.

4.1.2. Identification of Wheel Flats at Different Vehicle Speeds. The vehicle-track system is a nonlinear system. The nonlinear response of the ABA signal would be generated when the speed of the vehicle changes. In the literature [1], Zhai pointed out that the wheel-rail force of the vehicle with wheel flats is related to the change of the vehicle speed. Therefore, in order to analyze the influence of the change of vehicle speed on the vibration response of the vehicle system, the ABA signals are calculated in the speed of 80km/h, 90km/h, 100km/h, 110km/h, 120km/h, 130km/h, 140km/h, 150km/h, and 160km/h, respectively. Here, the length of wheel flat is 50mm and orbital excitation isn't considered. The ABA are shown in Figure 6(a). The maximum ABA are shown in Figure 6(b). The faster the vehicle runs, the smaller the ABA caused by the wheel flat is. The maximum acceleration decreases approximately linearly with the increase of vehicle speed.

The Hilbert envelope spectrums of $\boldsymbol{IMF_1}$ obtained by the same method at different vehicle speeds are shown in Figure 7(a). The sums of the Hilbert envelope spectrum of the $\boldsymbol{IMF_1}$-$\boldsymbol{IMF_3}$ obtained from the vibration signal are shown in Figure 7(b). In Figure 7, the vibration frequency of the wheel flat can be recognized from the ABA signals at different speeds. The decomposition results fluctuate near the theoretical frequency at different speeds, as shown in Table 2.

Effects of vehicle speed on amplitude of Hilbert envelope spectrum are shown in Figure 8. In Figure 8, the maximum amplitudes of the $\boldsymbol{IMF_1}$**'s** Hilbert envelope spectrum appear at the speed of 80km/h, while the maximum amplitudes of the sum of Hilbert envelope spectrum of the first three orders IMF appear at the speeds 80km/h and 100km/h.

Except for 90km/h, the variation laws of maximum acceleration are basically consistent with the effects of vehicle speed on the maximum ABA, as shown in Figure 7. There are three factors which would affect the decomposition results. Firstly, the faster the vehicle runs, the smaller the ABA caused by the wheel flat with same length is. However, the maximum amplitude difference of the ABA caused by the wheel flats with same length at the different speeds is small. Secondly, the ABA caused by the wheel flat is superimposed by that of the random irregularity of the track. The difference is caused by the random irregularity stimulation of the track. Thirdly, the same time sampling frequency corresponding to the spatial sampling frequency at different speeds is not consistent; that is, the numbers of sampling points are not consistent at different speeds.

4.2. Dual Wheel Flats

4.2.1. Identification of Wheel Flats with Different Lengths. Without orbital stimulation, the wheel has dual flats with 180° phase difference. The response curves of the vertical ABA are shown in Figure 9. The length of one flat is varied (10mm, 20mm, 30mm, 40mm, and 50mm) and the other has a fixed

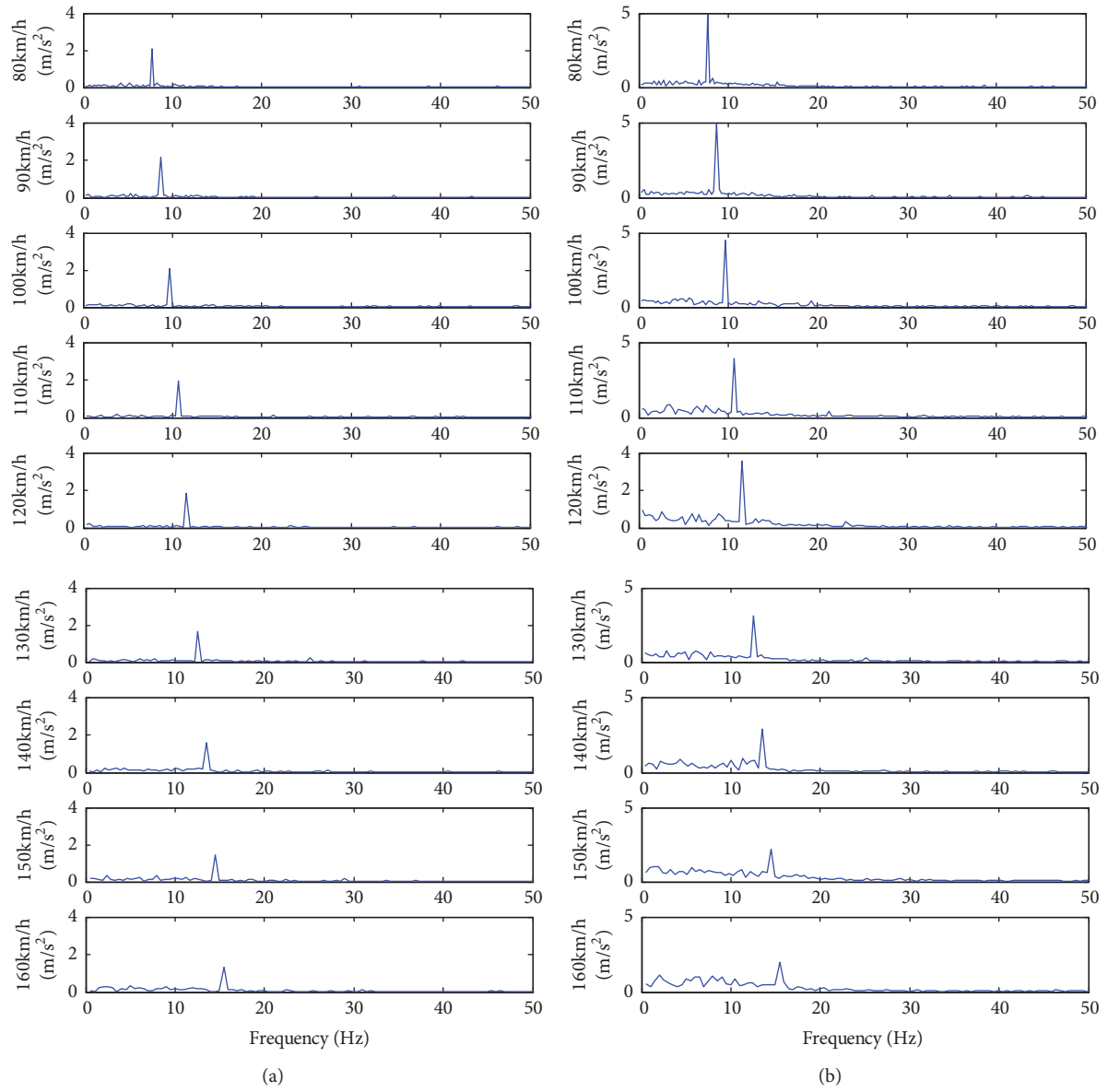

Figure 7: Hilbert envelope spectrum based on EMD with single flat having different speeds. (a) Hilbert envelope spectrum of IMF1 with different vehicle speeds. (b) The sum of Hilbert envelope spectrum of IMF1-IMF3 with different vehicle speeds.

Table 2: Effects of vehicle speeds on Hilbert envelope spectrum amplitude with single flat.

Speed (km/h)	Theoretical frequency (Hz)	Actual frequency (Hz)	Amplitude of IMF1Hilbert envelope spectrum (m/s^2)	Sum of Hilbert envelope spectrum amplitude of IMF1-IMF3 (m/s^2)
80	7.7307	7.7316	2.7589	4.8903
90	8.6970	8.6964	1.6721	3.7488
100	9.6633	9.6628	1.7595	4.8029
110	10.6297	10.6281	1.7345	4.5039
120	11.5960	11.5861	1.7944	3.6251
130	12.5623	12.5612	1.5507	2.8009
140	13.5287	13.5281	1.0633	2.5875
150	14.4950	14.4949	0.9039	2.1588
160	15.4613	15.4607	0.7424	1.8348

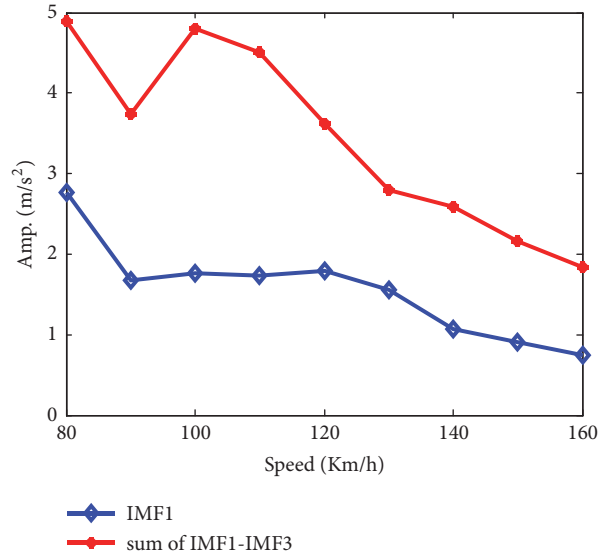

Figure 8: Effects of vehicle speed on Hilbert envelope spectrum amplitude with single flat.

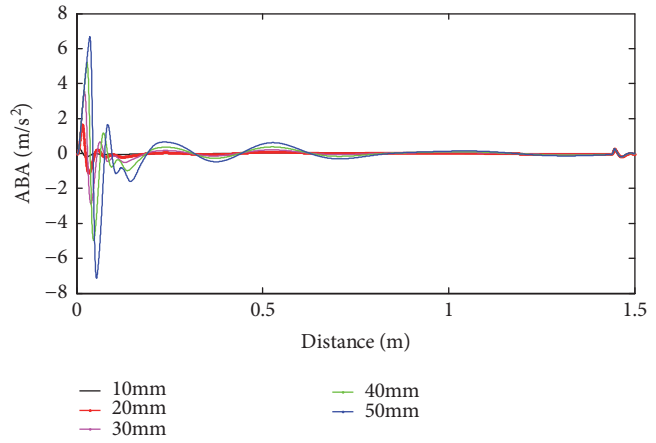

Figure 9: Vertical ABA with different dual flats and no orbit disturbance (V=100km/h).

length of 10mm. Similar to the result stimulated by single flat, the longer the wheel flat is, the larger the ABA is at the same vehicle speed. The two-flat scar with same phase difference will impact on the same location of track.

When the speed is 100km/h, the vertical ABA response curves, which are stimulated by dual flats and the American six-grade track irregularity, are shown in Figure 10. When the length of the wheel flat is small, the impact caused by the small wheel flat is submerged in the vibration response, which is resulted in the random irregularity of track. The theoretical impact frequency is still 9.6633Hz because the phase difference between the double flats on the same wheel is fixed.

The ABA signals stimulated by two flats are decomposed by EMD, and the first three orders (IMF_1-IMF_3) of the Hilbert envelope spectrums are calculated. Hilbert envelope spectrums of IMF_1 are shown in Figure 11(a), and the sums of first three orders (IMF_1-IMF_3) Hilbert envelope spectrum are shown in Figure 11(b). It can be concluded from Figure 11 that the Hilbert envelope spectrums of IMF_1 have better decomposition effect. The frequencies of flats can be identified accurately when the system is stimulated by dual wheel flats. The frequencies of the corresponding wheel flat are shown in Table 3. Similarly, both the amplitudes of Hilbert envelope spectrum of IMF_1 and the sums of Hilbert envelope spectrum amplitude of the first three intrinsic modes increase with the growth of flat length.

From Tables 1 and 3, the amplitudes of the envelope spectrum at 20mm, 30mm, 40mm, and 50mm flat length are larger than the amplitude of single flat. Because the length of the wheel flat is less than 10mm, the vibration caused by the flat is submerged in the random irregularity of the track. And its amplitude is slightly lower than that of the single flat, while the frequency of the flat can still be identified accurately. Effects of flat length on the amplitude of Hilbert envelope spectrum with dual flats are shown in Figure 12.

4.2.2. Identification of Wheel Flats at Different Vehicle Speeds. Through the method, the vehicle ABA signals with double flats are decomposed. The phase difference is 180°. The

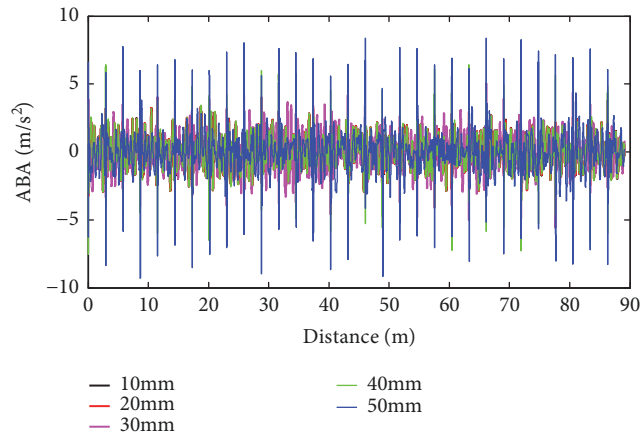

Figure 10: Vertical ABA with dual flats and American six-grade track irregularity (V=100km/h).

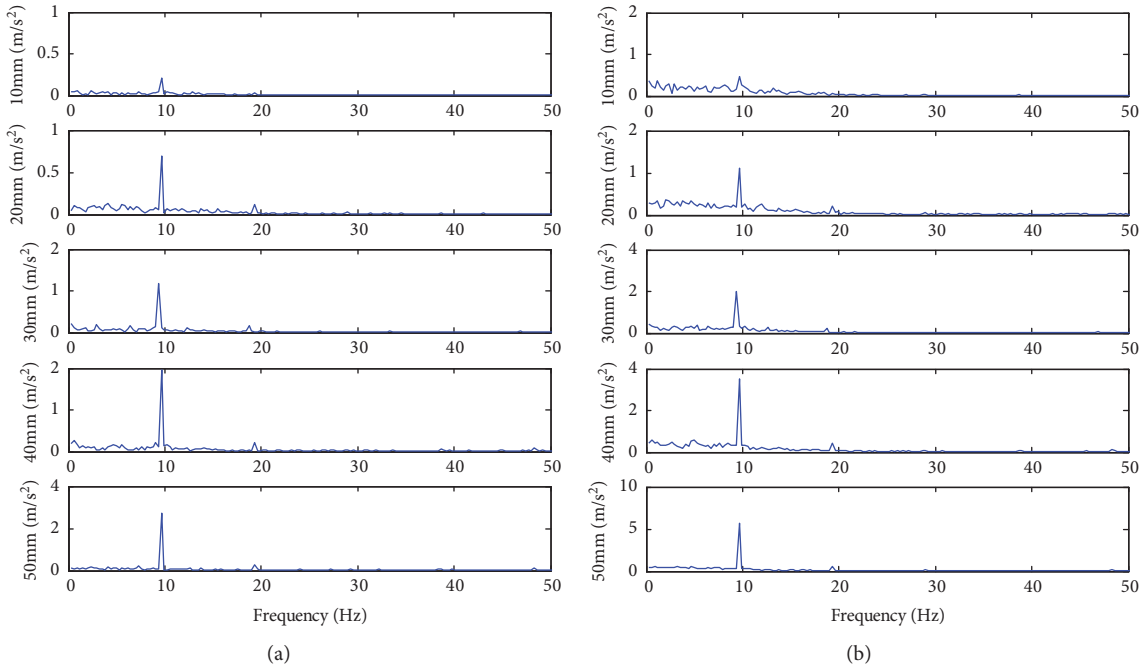

Figure 11: Hilbert envelope spectrum based on EMD with dual flats. (a) Hilbert envelope spectrum of IMF1 with different length flats. (b)The sum of Hilbert envelope spectrum of IMF1-IMF3 of the flat with different length flats.

results using EMD-Hilbert envelope spectrum are shown in Figure 13. Similar to the single flat excitations, the frequencies of the ABA stimulated by wheel flats at different speeds are also identified by this method. It indicates that this method could identify single or double flats at different speeds. The maximum amplitudes of the Hilbert enveloped spectrum of $\boldsymbol{IMF_1}$ and the maximum amplitudes of the sums of the first three-order $\boldsymbol{IMF}$ envelope spectrum are shown in Table 4. The faster the vehicle speed is, the smaller the maximum amplitude of the $\boldsymbol{IMF_1}$'s envelope spectrum is and the smaller the sum of maximal amplitude of the first three-order $\boldsymbol{IMF}$ envelope spectrum is. The change of maximum amplitude of the $\boldsymbol{IMF_1}$'s envelope spectrum is not of significant difference with the decrease of velocity.

As shown in Figure 14, the faster the speed of the vehicle, the smaller the maximal amplitude of the $\boldsymbol{IMFI}$'s Hilbert envelope spectrum, under the same length of the flats. And the amplitude maximum is approximate linear relationship with the vehicle speed. However, due to the nonlinearity of vehicle system, the decomposition results of ABA are more significant than that of single flat excitation. When the vehicle speed is 80km/h and 90km/h, the amplitude of Hilbert envelope spectrum is the largest. At this time, the vibration response of vehicle system stimulated by flat is more sufficient than that of track random irregularity. It is easier to identify the flat frequency.

4.2.3. Identification of Wheel Flats with Different Phase Differences. For the purpose to discuss the validity of this

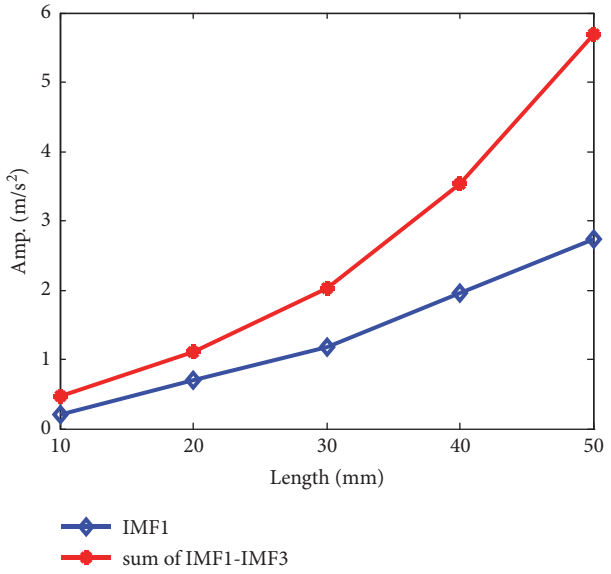

Figure 12: Effects of flat length on Hilbert envelope spectrum amplitude with dual flats.

Table 3: Effects of flat length on Hilbert envelope spectrum amplitude with dual flats.

Flat length (mm)	Actual frequency (Hz)	Amplitude of IMF1Hilbert envelope spectrum (m/s^2)	Sum of Hilbert envelope spectrum amplitude of IMF1-IMF3 (m/s^2)
10	9.658	0.2054	0.4778
20	9.658	0.6932	1.1056
30	9.661	1.1848	2.0216
40	9.658	1.9579	3.5301
50	9.658	2.7344	5.6904

Table 4: Effects of vehicle speeds on Hilbert envelope spectrum amplitude with dual flats.

Speed (km/h)	Theoretical frequency (Hz)	Actual frequency (Hz)	Amplitude of IMF1Hilbert envelope spectrum (m/s^2)	Sum of Hilbert envelope spectrum amplitude of IMF1-IMF3 (m/s^2)
80	7.7307	7.7304	2.0983	4.9091
90	8.6970	8.6964	2.1515	4.9308
100	9.6633	9.6618	2.0665	4.5056
110	10.6297	10.6293	1.9628	3.9305
120	11.5960	11.5861	1.8422	3.5623
130	12.5623	12.5612	1.6490	3.1250
140	13.5287	13.5253	1.5864	2.9059
150	14.4950	14.4844	1.4668	2.2312
160	15.4613	15.4607	1.3247	1.9555

method, we choose two flats with phase differences of 45°, 90°, 135°,180°, 225°, 270°, and 315°, respectively. Figure 15 is the decomposition results. The vehicle system has dual flats with different phase difference. The vehicle speed is 100km/h and the two flats lengths are 50mm and 10mm, respectively. As shown in Figure 15, the method proposed in this paper can also obtain ideal results. The actual frequency is 9.6628 Hz and the error is 0.005%. Effects of phase difference on Hilbert envelope spectrum amplitude with dual flats are shown in Table 5.

Effects of phase difference on Hilbert envelope spectrum amplitude are shown in Figure 16. When the phase difference is 180°, the maximum amplitude of the envelope spectrum is the smallest. That is to say, the influence of the two flats on each other is the smallest at this time. The smaller the phase difference of the flats is, the larger the maximal amplitude of the envelope spectrum is. The dual wheel flat causes the nonlinear superposition of the vibration response. When the absolute values of the phase differences of two flat are identical, the ABAs caused by the large flat followed by a small

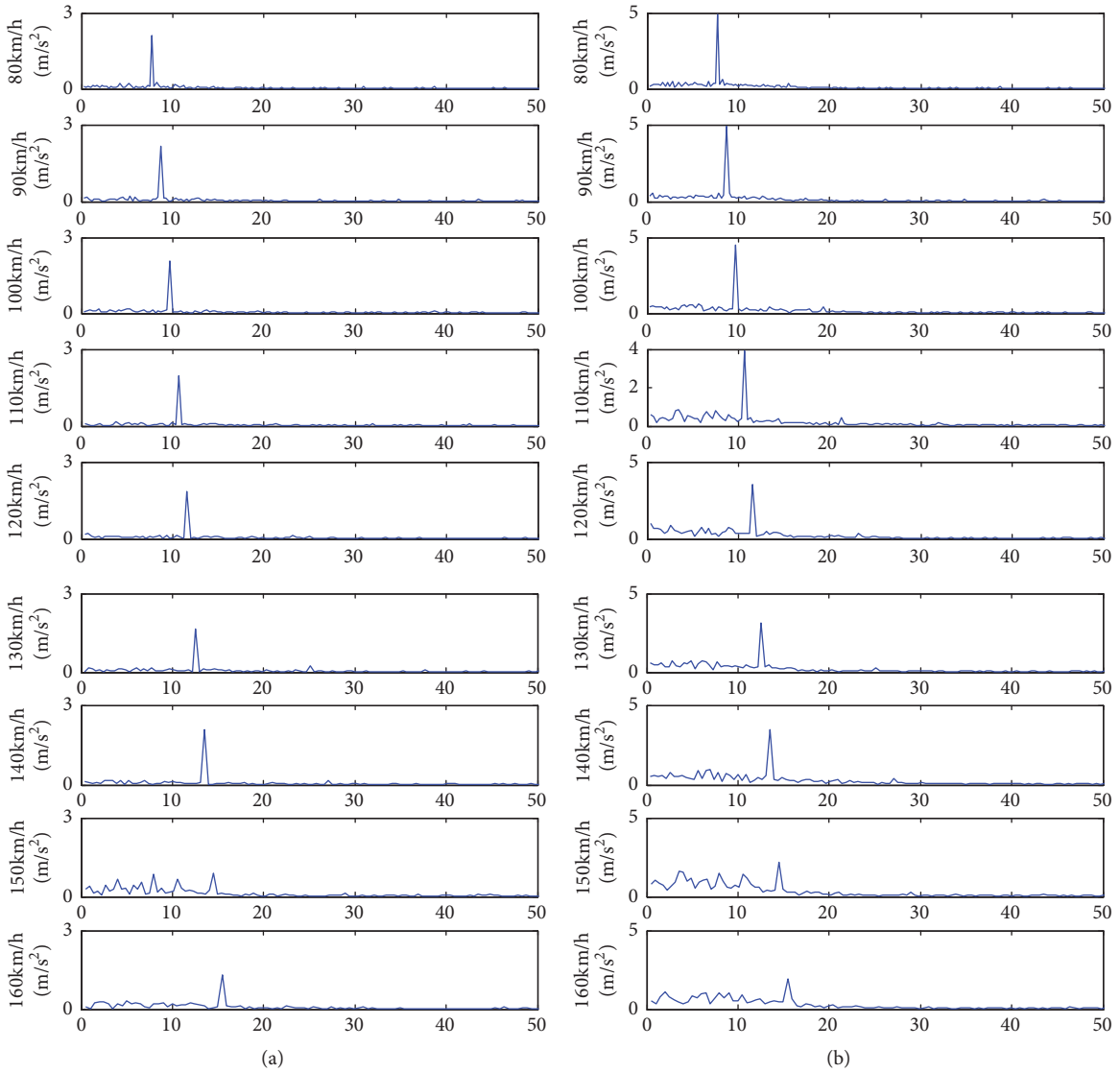

Figure 13: Hilbert envelope spectrum based on EMD with dual flat in different speeds (phase difference=180°). (a) Hilbert envelope spectrum of IMF1 with different vehicle speeds. (b) The sum of Hilbert envelope spectrum of IMF1-IMF3 with different vehicle speeds.

Table 5: Effects of phase difference on Hilbert envelope spectrum amplitude with dual flats.

Phase different (°)	Theoretical frequency (Hz)	Actual frequency (Hz)	Amplitude of IMF1Hilbert envelope spectrum (m/s^2)	Sum of Hilbert envelope spectrum amplitude of IMF1-IMF3 (m/s^2)
45	9.6633	9.6628	3.9828	6.4230
90	9.6633	9.6628	3.5167	6.8270
135	9.6633	9.6628	2.1765	4.7171
180	9.6633	9.6628	2.0034	4.6479
225	9.6633	9.6628	2.0981	4.6475
270	9.6633	9.6628	2.3238	2.3238
315	9.6633	9.6628	2.7706	2.7706

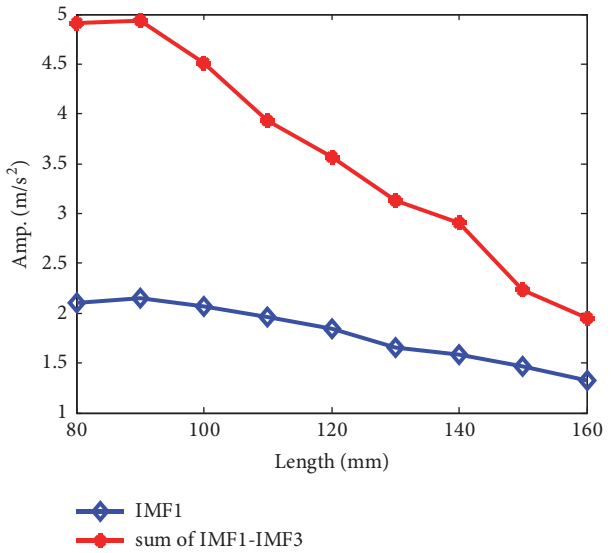

Figure 14: Effects of vehicle speed on Hilbert envelope spectrum amplitude with dual flats.

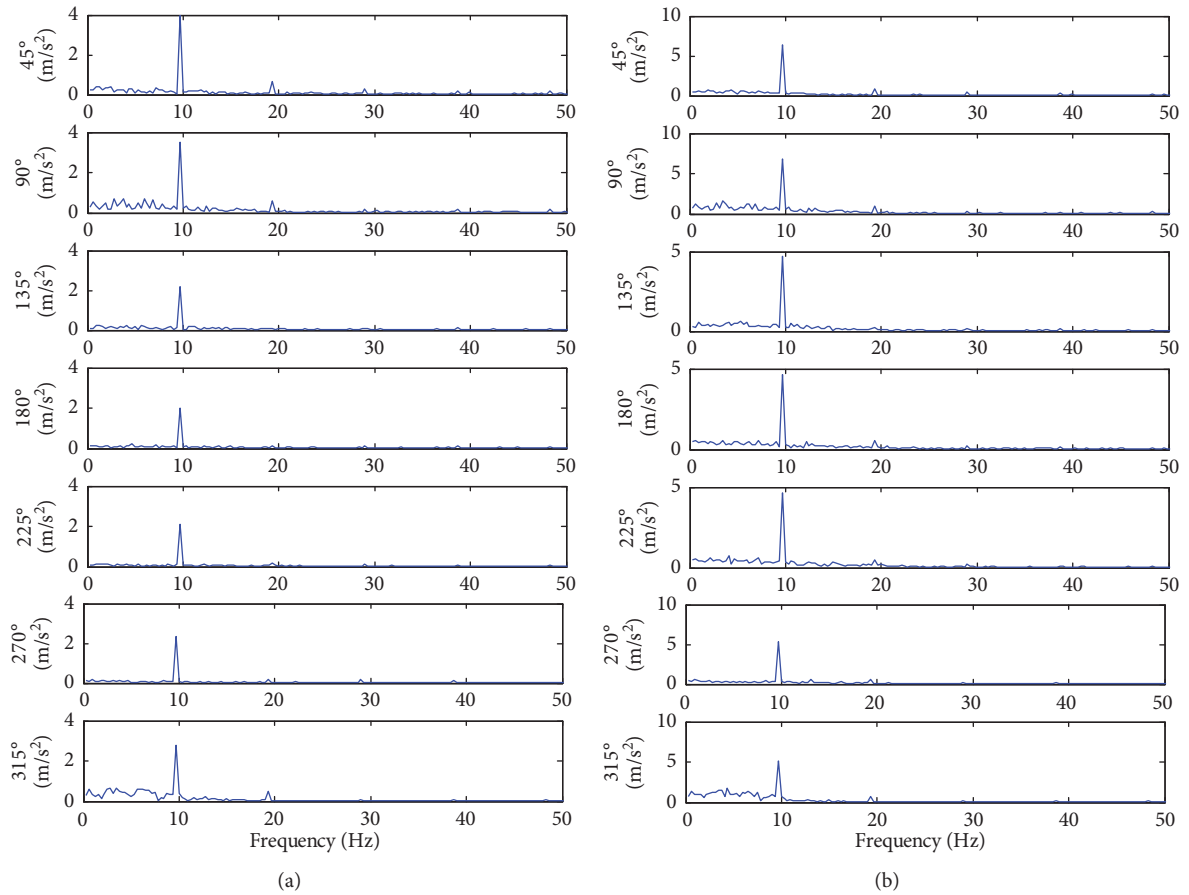

Figure 15: Hilbert envelope spectrum based on EMD with dual flats having different phase differences (V=100km/h). (a) Hilbert envelope spectrum of IMF1 with different phase differences. (b) The sum of Hilbert envelope spectrum of IMF1-IMF3 of the flat with different phase differences.

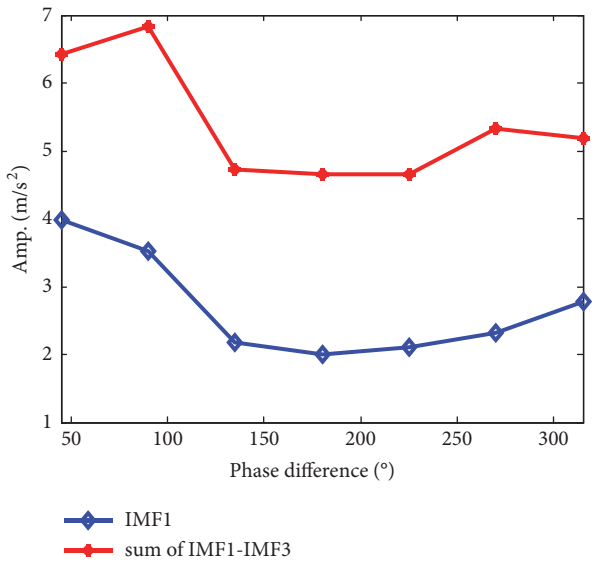

Figure 16: Effects of phase difference on Hilbert envelope spectrum amplitude with dual flats.

flat are significantly greater than that of the small flat followed by a large flat. The reason is the nonlinearity of vehicle-track coupling system.

5. Conclusion

Although dynamic action of wheel-rail can directly reflect the dynamic effect of vehicle on track, the dynamic wheel-rail force also includes the impact force caused by the high frequency contact vibration between the vehicle un-sprung weight and the rail mass. Therefore, the axle box acceleration signal is used in this paper to identify the wheel flats.

In this paper, the Injury Model of Wheel Flat is established. The axle box acceleration signals are obtained when the vehicle is stimulated at different speeds, different lengths of wheel flat, and different phase differences between two flats. The Hilbert envelope spectrum based on EMD is applied to axle box acceleration signals in this paper. The results show that this method can effectively extract the characteristics of the axle box vertical vibration response caused by the wheel flats in the complex operating environment. This method has a good effect. Because the result of decomposition is not affected by the length of flat and the change of speed, its performance is stable. The flat length could be estimated by the amplitude corresponding to the flat frequency components. The fault diagnosis of wheel flat could be accomplished. As far as the cost concern, the cost of this method is low, the maintenance is simple, and the influence on the line is small. Therefore, the vibration acceleration detection method is suitable for the digital railway development requirements in China. This method is worthy of further research and further promotion in the field of rail transit.

Data Availability

The data in the paper is generated by a simulation model of vehicle-track coupling system.

Conflicts of Interest

The authors declare that they have no conflicts of interest.

Acknowledgments

This study was partly supported by Key Fund Project of Sichuan Provincial Education Department (No. 16ZA0153) and ChunHui Project of Ministry of Education of China (No. Z2014077).

References

[1] W. Zhai M, Q. Wang C, and Z. Lu W, "Dynamic effects of vehicles on tracks in the case of raising train speeds," *Proceedings of the Institution of Mechanical Engineers Part F Journal of Rail & Rapid Transit*, vol. 215, no. 2, pp. 125–135, 2001.

[2] R. U. A. Uzzal, A. K. W. Ahmed, and S. Rakheja, "Analysis of pitch plane railway vehicle-track interactions due to single and multiple wheel flats," *Proceedings of the Institution of Mechanical Engineers, Part F: Journal of Rail and Rapid Transit*, vol. 223, no. 4, pp. 375–390, 2009.

[3] D. Lyon, "The calculation of track forces due to the dipped rail joints, wheel flats and rail welds," *The Second ORE Colloquium on Technical Computer Programs*, 1972.

[4] S. G. Newton and R. A. Clark, "An investigation into the dynamic effects on the track of wheelflats on railway vehicles," *Journal of Mechanical Engineering Science*, vol. 21, no. 4, pp. 287–297, 1979.

[5] A. Alemi, F. Corman, and G. Lodewijks, "Condition monitoring approaches for the detection of railway wheel defects," *Proceedings of the Institution of Mechanical Engineers, Part F: Journal of Rail and Rapid Transit*, vol. 231, no. 8, pp. 961–981, 2017.

[6] Z. Wanming, *Vehicle-Track Coupling Dynamics*, Science Press, 2007.

[7] M. Pau, "Ultrasonic waves for effective assessment of wheel-rail contact anomalies," *Proceedings of the Institution of Mechanical*

Engineers, Part F: Journal of Rail and Rapid Transit, vol. 219, no. 2, pp. 79–90, 2005.

[8] R. Pohl, A. Erhard, H.-J. Montag, H.-M. Thomas, and H. Wüstenberg, "NDT techniques for railroad wheel and gauge corner inspection," *NDT & E International*, vol. 37, no. 2, pp. 89–94, 2004.

[9] M. Pau, B. Leban, and A. Baldi, "Simultaneous subsurface defect detection and contact parameter assessment in a wheel-rail system," *Wear*, vol. 265, no. 11-12, pp. 1837–1847, 2008.

[10] M. B. Marshall, R. Lewis, R. S. Dwyer-Joyce, U. Olofsson, and S. Björklund, "Experimental characterization of wheel-rail contact patch evolution," *Journal of Tribology*, vol. 128, no. 3, pp. 493–504, 2006.

[11] C. Peng, K. Fan, M. Song et al., "Automatic railway wheelset inspection system by using ultrasonic technique," in *Proceedings of the Seventh International Symposium on Precision Engineering Measurements and Instrumentation*, p. 83212C, Yunnan, China.

[12] A. G. Verkhoglyad, I. N. Kuropyatnik, V. M. Bazovkin, and G. L. Kuryshev, "Infrared diagnostics of cracks in railway carriage wheels," *Russian Journal of Nondestructive Testing*, vol. 44, no. 10, pp. 664–668, 2008.

[13] Y. Yao, S. Sfarra, C. Ibarra-Castanedo, R. You, and X. P. V. Maldague, "The multi-dimensional ensemble empirical mode decomposition (MEEMD): An advanced tool for thermographic diagnosis of mosaics," *Journal of Thermal Analysis and Calorimetry*, vol. 128, no. 3, pp. 1841–1858, 2017.

[14] N. Rajic, "Principal component thermography for flaw contrast enhancement and flaw depth characterisation in composite structures," *Composite Structures*, vol. 58, no. 4, pp. 521–528, 2002.

[15] H. Zhang, S. Sfarra, K. Saluja et al., "Non-destructive Investigation of Paintings on Canvas by Continuous Wave Terahertz Imaging and Flash Thermography," *Journal of Nondestructive Evaluation*, vol. 36, no. 2, 2017.

[16] S. J. Kwon, J. W. Seo, D. H. Lee, and W. J. You, "Detection of sub-surface crack in railway wheel using a new sensing system," in *Proceedings of the SPIE Smart Structures and Materials + Nondestructive Evaluation and Health Monitoring*, p. 79833A, San Diego, California, USA.

[17] Z. H. Zurek, "Magnetic monitoring of the fatigue process of the rim material of railway wheel sets," *NDT & E International*, vol. 39, no. 8, pp. 675–679, 2006.

[18] J. Hwang, J. Lee, and S. Kwon, "The application of a differential-type Hall sensors array to the nondestructive testing of express train wheels," *NDT & E International*, vol. 42, no. 1, pp. 34–41, 2009.

[19] A. Johansson and J. C. Nielsen, "Out-of-round railway wheels—wheel-rail contact forces and track response derived from field tests and numerical simulations," *Proceedings of the Institution of Mechanical Engineers, Part F: Journal of Rail and Rapid Transit*, vol. 217, no. 2, pp. 135–146, 2006.

[20] C. C. Lai, J. C. P. Kam, D. C. C. Leung et al., "Development of a Fiber-Optic Sensing System for Train Vibration and Train Weight Measurements in Hong Kong," *Journal of Sensors*, vol. 2012, Article ID 365165, 7 pages, 2012.

[21] A. Bracciali and G. Cascini, "Detection of corrugation and wheelflats of railway wheels using energy and cepstrum analysis of rail acceleration," *Proceedings of the Institution of Mechanical Engineers, Part F: Journal of Rail and Rapid Transit*, vol. 211, no. 2, pp. 109–116, 1997.

[22] D. Skarlatos, K. Karakasis, and A. Trochidis, "Railway wheel fault diagnosis using a fuzzy-logic method," *Applied Acoustics*, vol. 65, no. 10, pp. 951–966, 2004.

[23] V. Belotti, F. Crenna, R. C. Michelini, and G. B. Rossi, "Wheel-flat diagnostic tool via wavelet transform," *Mechanical Systems and Signal Processing*, vol. 20, no. 8, pp. 1953–1966, 2006.

[24] M. L. Lee and W. K. Chiu, "Determination of railway vertical wheel impact magnitudes: Field trials," *Structural Health and Monitoring*, vol. 6, no. 1, pp. 49–65, 2007.

[25] N. Thakkar, J. A. Steel, R. Reuben, G. Knabe, D. Dixon, and R. Shanks, "Monitoring of Rail-Wheel Interaction Using Acoustic Emission (AE)," *Advanced Materials Research*, vol. 13-14, pp. 161–168, 2006.

[26] R. S. Dwyer-Joyce, C. Yao, R. Lewis, and H. Brunskill, "An ultrasonic sensor for monitoring wheel flange/rail gauge corner contact," *Proceedings of the Institution of Mechanical Engineers, Part F: Journal of Rail and Rapid Transit*, vol. 227, no. 2, pp. 188–195, 2013.

[27] B. Frankenstein, D. Hentschel, E. Pridoehl, and F. Schubert, "Hollow shaft integrated health monitoring system for railroad wheels," in *Proceedings of the Advanced Sensor Technologies for Nondestructive Evaluation and Structural Health Monitoring*, pp. 46–55, USA, March 2005.

[28] S. Jia and M. Dhanasekar, "Detection of rail wheel flats using wavelet approaches," *Structural Health and Monitoring*, vol. 6, no. 2, pp. 121–131, 2007.

[29] B. Liang, S. D. Iwnicki, Y. Zhao, and D. Crosbee, "Railway wheel-flat and rail surface defect modelling and analysis by time-frequency techniques," *Vehicle System Dynamics*, vol. 51, no. 9, pp. 1403–1421, 2013.

[30] B. Liang, S. Iwnicki, A. Ball, and A. E. Young, "Adaptive noise cancelling and time-frequency techniques for rail surface defect detection," *Mechanical Systems and Signal Processing*, vol. 54-55, pp. 41–51, 2015.

[31] V. Kumar, V. Rastogi, and P. Pathak, "Dynamic analysis of vehicle–track interaction due to wheel flat using bond graph," *Proceedings of the Institution of Mechanical Engineers, Part K: Journal of Multi-body Dynamics*, vol. 232, no. 3, pp. 398–412, 2017.

[32] A. Matsumoto, Y. Sato, H. Ohno et al., "A new measuring method of wheel-rail contact forces and related considerations," *Wear*, vol. 265, no. 9-10, pp. 1518–1525, 2008.

[33] Y. Chen, X. Wang, Y. Zhang, and Z. Xing, "Fault Diagnosis of Train Wheels Based on Empirical Mode Decomposition Generalized Energy," in *Proceedings of the 3rd International Conference on Electrical and Information Technologies for Rail Transportation (EITRT) 2017*, vol. 483 of *Lecture Notes in Electrical Engineering*, pp. 15–25, Springer Singapore, Singapore, 2018.

[34] Y. Li, J. Liu, and Y. Wang, "Railway Wheel Flat Detection Based on Improved Empirical Mode Decomposition," *Shock and Vibration*, vol. 2016, 2016.

[35] L. Lin, Y. Wang, and H. Zhou, "Iterative filtering as an alternative algorithm for empirical mode decomposition," *Advances in Adaptive Data Analysis (AADA)*, vol. 1, no. 4, pp. 543–560, 2009.

[36] A. Cicone, J. Liu, and H. Zhou, "Adaptive local iterative filtering for signal decomposition and instantaneous frequency analysis," *Applied and Computational Harmonic Analysis* , vol. 41, no. 2, pp. 384–411, 2016.

[37] N. E. Huang, Z. Shen, S. R. Long et al., "The empirical mode decomposition and the Hilbert spectrum for nonlinear and

non-stationary time series analysis," *Proceedings A*, vol. 454, pp. 903–995, 1998.

[38] E. Huang N, "Computer Implemented Empirical Mode Decomposition Method, Apparatus, and Article of Manufactur," *Provisional Application*, vol. 5, pp. 983-162, 1999.

[39] H. Jiang and L. Jianhui, "Analysis of vibration characteristics of vehicle-track vertically coupling system excited by harmonic waves based on improved EMD," *Journal of Information Hiding and Multimedia Signal Processing*, vol. 9, no. 5, pp. 1156–1169, 2018.

[40] W. Futian, *Vehicle System Dynamics*, China Railway Publishing House, 1994.